Neurovascular crosstalk between interneurons and capillaries is required for vision

Yoshihiko Usui,[1] Peter D. Westenskow,[1,2] Toshihide Kurihara,[1] Edith Aguilar,[1] Susumu Sakimoto,[1] Liliana P. Paris,[1] Carli Wittgrove,[1] Daniel Feitelberg,[1] Mollie S.H. Friedlander,[1] Stacey K. Moreno,[1] Michael I. Dorrell,[2] and Martin Friedlander[1]

[1]Department of Cell and Molecular Biology, The Scripps Research Institute, La Jolla, California, USA. [2]Lowy Medical Research Institute, La Jolla, California, USA.

Functional interactions between neurons, vasculature, and glia within neurovascular units are critical for maintenance of the retina and other CNS tissues. For example, the architecture of the neurosensory retina is a highly organized structure with alternating layers of neurons and blood vessels that match the metabolic demand of neuronal activity with an appropriate supply of oxygen within perfused blood. Here, using murine genetic models and cell ablation strategies, we have demonstrated that a subset of retinal interneurons, the amacrine and horizontal cells, form neurovascular units with capillaries in 2 of the 3 retinal vascular plexuses. Moreover, we determined that these cells are required for generating and maintaining the intraretinal vasculature through precise regulation of hypoxia-inducible and proangiogenic factors, and that amacrine and horizontal cell dysfunction induces alterations to the intraretinal vasculature and substantial visual deficits. These findings demonstrate that specific retinal interneurons and the intraretinal vasculature are highly interdependent, and loss of either or both elicits profound effects on photoreceptor survival and function.

Introduction

Neurovascular units consist of varying combinations of neurons, glia, pericytes, and the extracellular matrix, which interact with endothelial cells to regulate local blood supply. The importance of the neurovascular unit for maintaining local functionality and homeostasis in the CNS has recently received increased attention, since defects in neurovascular units are associated with a variety of CNS diseases, including stroke, Alzheimer's disease, Parkinson's disease, amyotrophic lateral sclerosis, cerebral palsy, migraines, and mood disorders (1, 2). Therefore, learning how neurovascular units are established and maintained may be crucial for understanding the basis of a host of neurodegenerative diseases and for developing therapeutic strategies for treating them.

The retina is an excellent model system for studying neurovascular interactions in the CNS, since formation of the retinal vasculature and neurons occurs in well-characterized, consistent, and reproducible temporal and spatial patterns. In addition, retinal neurovascular units can be directly visualized and assessed functionally using highly sensitive imaging modalities (3, 4). Neuronal and vascular networks in the sensory retina are organized in a highly stratified and functional architecture, although the full extent of their integration is not completely understood. Phototransduction, the process of generating electrical signals from captured photons, occurs in rod and cone photoreceptor cells in the outer retina. Bipolar cells in the inner nuclear layer (INL) transmit the visual signals from the photoreceptors to the retinal ganglion cells, which send the integrated signal to the visual cortex. The INL also contains laterally interconnecting amacrine and horizontal cells that localize at opposite margins of the INL and form homotypic and heterotypic connections within the inner plexiform layer (IPL) and outer plexiform layer (OPL), respectively. Horizontal cells provide inhibitory feedback for cone-driven pathways, and amacrine cells have diverse physiologies and exhibit multifaceted connectivity throughout the IPL that allows them to preprocess and integrate visual signals and interpose temporal cues. In this study, we demonstrate another function for these retinal interneurons: promoting photoreceptor homeostasis through maintenance of the vasculature.

The vascular networks in the retina are architecturally optimized, albeit in species-specific manners, to sustain the extreme metabolic demands of retinal neurons — in particular, the photoreceptors. In primates and mice, the intraretinal vasculature consists of 3 interconnected parallel vascular plexus layers in the plexiform layers of the retina. In mice, the retinal vasculature forms as endothelial cells migrate from the optic nerve onto the retinal surface at birth and progress radially to form the superficial (or inner) plexus (4). Around postnatal day 7 (P7), sprouting vessels descend and advance into the OPL, where they establish the deep plexus. At P11–P12 stages, sprouting vessels from the deep plexus ascend into the IPL and ramify to form the intermediate plexus. The proangiogenic stimuli that direct formation of the intermediate and deep (or outer) plexus layers are not completely understood and are likely distinct (5). It has been suggested that oxygen and nutrient insufficiencies, induced as retinal neurons are born and mature, activate hypoxic responses via von Hippel-Lindau/Hypoxia-inducible factor (VHL/HIF) signaling pathways that drive the expression of proangiogenic factors, including VEGF and EPO (6, 7). This concept is supported by 2 key pieces of evidence: HIF-1α is detectable at high levels in the developing retina, and conditional deletion in virtually all retinal cells of the murine peripheral retina prevents formation of the interme-

Authorship note: Yoshihiko Usui and Peter D. Westenskow contributed equally to this work.
Conflict of interest: The authors have declared that no conflict of interest exists.
Submitted: December 3, 2014; **Accepted:** March 19, 2015.
Reference information: *J Clin Invest*. 2015;125(6):2335–2346. doi:10.1172/JCI80297.

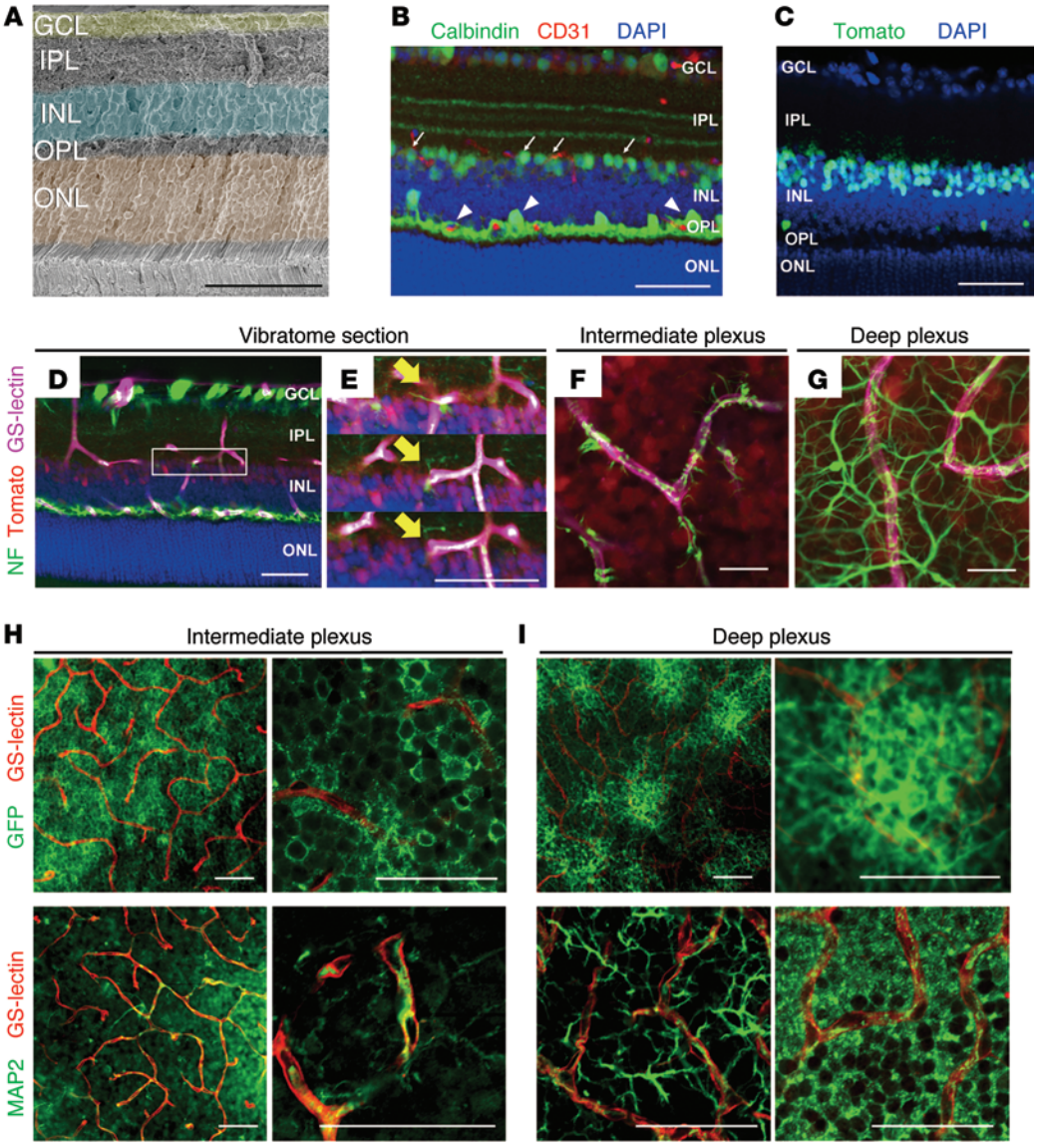

Figure 1. Amacrine and horizontal cells form neurovascular units with the intraretinal capillaries. (**A**) Pseudocolored cross section of an adult murine retina. (**B**) Immunohistochemistry was used to identify putative neurovascular units between amacrine cells (arrows) or horizontal cells (arrowheads) with the vasculature using anti-calbindin (green), anti-CD31 (red), and DAPI (blue) in WT retinal cryosections at P23. (**C**) Cre recombination reporters label amacrine and horizontal cell nuclei in P23 *Ptf1a-Cre R26*$^{tdTomato/+}$ mice (tomato signal was pseudocolored green). (**D**–**I**) Amacrine (**D**–**F**) and horizontal cell (**D** and **G**) neurites (NF-M labeled, green) associate with the intraretinal vasculature (GS-lectin, blue) as seen in thick cut (100 μm) sections (amacrine/horizontal nuclei, red). (**E**) Adjacent optical slices from the region of interest boxed in (**D**); arrows mark colocalization. (**F** and **G**) Flat-mounted P23 *Ptf1a-Cre R26*$^{tdTomato/+}$ retinas colabeled with anti-neurofilament and GS-lectin (endothelial cell marker). (**H** and **I**) Amacrine cell neurites are decorated with GFP in *Ptf1a-Cre R26*^{GFP} mice and can be observed in close proximity to GS-lectin–positive endothelial cells. Immunofluorescence for MAP2 in whole-mount retinas at P23 also reveals colocalization of amacrine and horizontal cell neurites with the intraretinal vasculature. Scale bars: 50 μm (**A**–**E**, **H**, and **I**); 20 μm (**F** and **G**).

diate plexus. (5, 6, 8). Inhibition of VEGF — which is transiently expressed throughout the developing INL — inhibits formation of the intraretinal vasculature (9, 10). While there is a clear role for VHL/HIF and VEGF in regulating intermediate plexus development, the cells in the INL that are responsible for regulating these factors have not been identified.

We observed extensive interactions between horizontal cells and capillaries of the deep plexus, and between amacrine cells and the intermediate vascular plexus in WT adult mice. Thus, both cell types are ideally localized to serve as metabolic and oxygen sensors in the retina, to activate angiogenesis during development through VHL/HIF/VEGF signaling, to provide structural and trophic support to the vasculature, and perhaps even to prevent pathological neurovascular remodeling. These functions may be critical, since destabilized vascular networks in the retina are associated with dramatic visual defects (11). There is growing evidence that blood vessels and proangiogenic mitogens contribute to the pathogenesis of multiple neurological diseases (1, 12). Therefore, it is important to understand the mechanisms of neurovascular crosstalk and vascular maintenance in the retina.

In this study, we utilized conditional gene deletion and cell ablation approaches to demonstrate that amacrine and horizontal

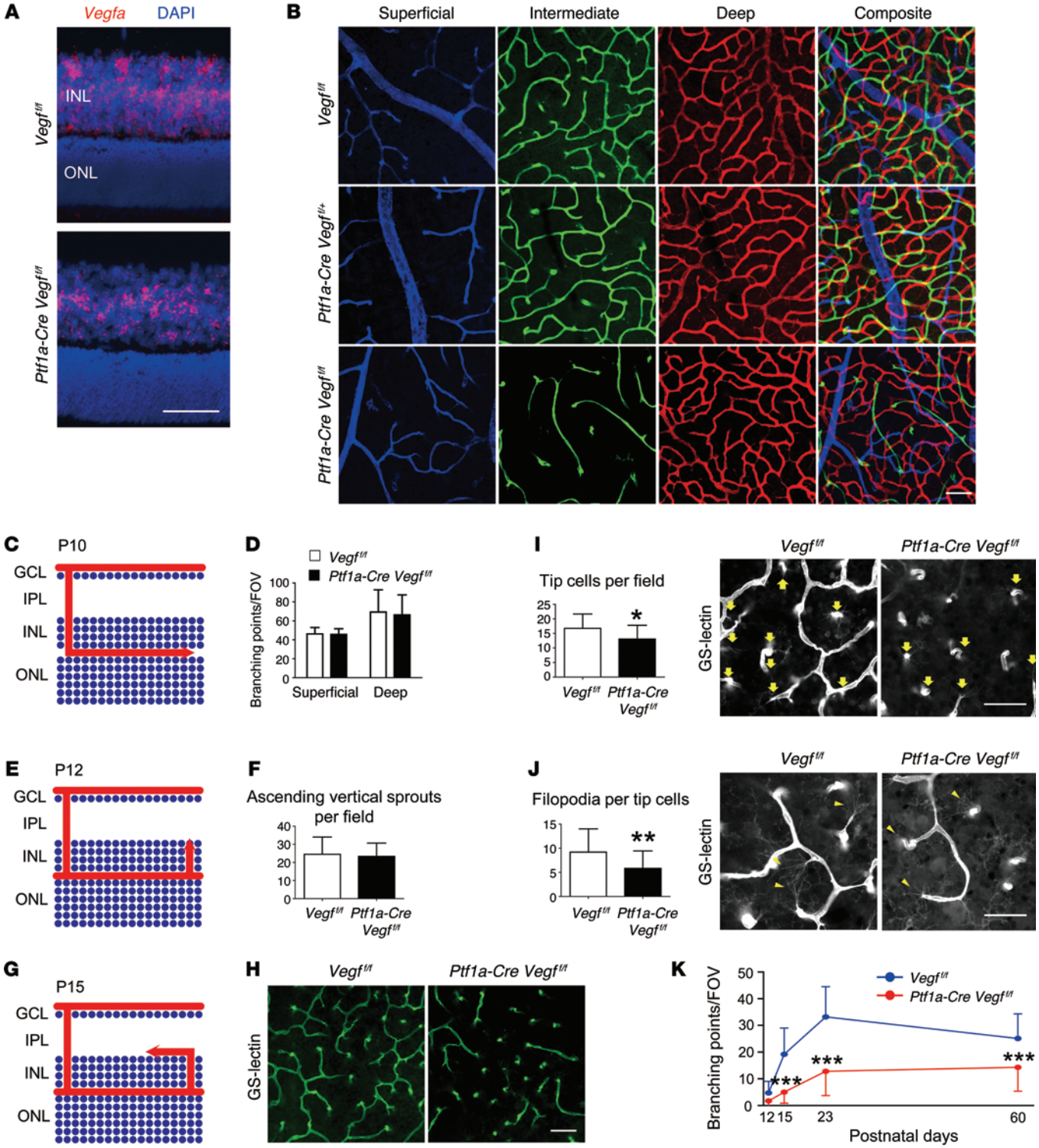

Figure 2. *Vegfa* deletion in amacrine and horizontal cells severely impairs intraretinal vasculature development. (**A**) In situ hybridization was performed on P12 *Vegf*$^{f/f}$ or *Ptf1a-Cre Vegf*$^{f/f}$ cryosectioned retinas with a *Vegfa* probe (counterstained with DAPI). (**B**) The intermediate plexus (green) is severely attenuated in P23 *Ptf1a-Cre Vegf*$^{f/f}$ compared with controls. (**C**) Schematic of deep plexus development in a P10-staged mouse. Arrow illustrates the lateral growth of blood vessels in the OPL. (**D**) The number of branching events in the superficial and deep plexuses of P10 *Vegf*$^{f/f}$ or *Ptf1a-Cre Vegf*$^{f/f}$ retinas were counted and plotted (n = 4). (**E**) Schematic of vertical sprouting events from the deep plexus in P12 retinas. Arrow illustrates the direction of vascular sprouting from the deep plexus to the IPL. (**F**) There are no differences in the numbers of ascending vertical sprouts of *Ptf1a-Cre Vegf*$^{f/f}$ in flat-mounted retinas compared with controls (*Vegf*$^{f/f}$) (n = 4). (**G**) Schematic of intermediate plexus development at P15. Arrow illustrates the lateral growth of blood vessels in the IPL. (**H**–**J**) GS-lectin–positive laterally expanding sprouts are fewer in number in P15 *Ptf1a-Cre Vegf*$^{f/f}$ mice due to a reduced number of tip cells (**I**; arrows) and filopodia (**J**; arrowheads) (n = 4–5). (**K**) The number of branching points in the intermediate plexus were counted, quantified, and plotted at P12, P15, P23, and P60 (n = 4–6). $^*P < 0.05$, $^{**}P < 0.01$, $^{***}P < 0.001$; 2-tailed Student's t tests. Error bars indicate mean ± SD. Scale bars: 50 μm (**A**, **B**, and **H**); 40 μm (**I** and **J**).

cells can regulate local blood supply in vivo and thereby promote photoreceptor homeostasis. We demonstrate that the key source of VEGF in the INL to regulate intermediate plexus development likely comes from the amacrine cells, and gain-of-function or loss-of-function of VEGF in amacrine cells induces marked defects in visual function and rod- and cone-driven signaling. These observations may have broad applicability for neurovascular unit physiology in the CNS and may also inform future therapies that target the neurovascular unit to treat not only blindness, but also a host of debilitating neurodegenerative and neurological diseases.

Results

Amacrine and horizontal cells form neurovascular units with capillaries in the intraretinal plexuses. The retinal neuronal and vascular networks are depicted in Figure 1A and Supplemental Figure 1 (supplemental material available online with this article; doi:10.1172/JCI80297DS1). P23 retinas were probed with specific markers for amacrine and horizontal cells (calbindin) and for endothelial cells (CD31) to identify putative neurovascular units. Immunohistochemistry analyses revealed that amacrine cell and horizontal cell dendrites appear to interact with CD31-positive intraretinal capillaries in the intermediate and deep plexuses in the IPL and OPL (arrows and arrowheads, respectively) (Figure 1B). To confirm the immunofluorescence findings, and since calbindin labels only a small percentage of amacrine cells, we utilized Cre/loxP transgenic-based approaches — with pancreas-specific transcription factor 1a-*Cre (Ptf1a-Cre*) mice — to genetically label amacrine and horizontal cells in the retina, and not bipolar cells or Müller glia (*Ptf1a-Cre R26*$^{tdTomato/+}$ and *Ptf1a-Cre R26*$^{GFP/+}$) (Figure 1C; Supplemental Figure 2, A–E; refs. 13, 14). We combined genetic labeling and immunofluorescence techniques to confirm that Cre-recombination occurs in amacrine cells by probing P23 *Ptf1a-Cre R26*$^{tdTomato/+}$ retinas with amacrine cell–specific antibodies (Supplemental Figure 2, B–D). Then we performed immunohistochemistry on P23 *Ptf1a-Cre R26*$^{tdTomato/+}$ retinas with antibodies that recognize the intermediate form of neurofilament (NF-M) — a marker for ganglion, amacrine, and horizontal cell axons (15) — or microtubule-associated protein 2 (MAP-2) — a marker for neuronal dendrites. Using this approach, we were able to more clearly visualize the extent of colocalization of the amacrine and horizontal cell arbors, and the vasculature in the IPL (Figure 1, D–F and H, and Supplemental Figure 2, F–H) and in the OPL (Figure 1, D, G, and I, and Supplemental Figure 2, F and H). Based on the findings that amacrine and horizontal cells interact extensively with the intraretinal capillaries, we hypothesized that amacrine and horizontal cells form neurovascular units in the 2 plexiform layers.

Amacrine cell– and horizontal cell–derived VEGF is essential for neurovascular-unit formation in the IPL. We first confirmed that mRNA for the proangiogenic cytokine *Vegfa* is broadly detectable in the INL at P12 when the intraretinal vasculature is developing (Figure 2A). To determine the contribution of amacrine cell– and horizontal cell–derived VEGF, we first combined floxed *Vegfa (Vegfa*$^{f/f}$*)*(16) and *Ptf1a-Cre* alleles in transgenic mice and analyzed the vascular phenotype. While the deletion of *Vegfa* from amacrine and horizontal cells substantially reduced *Vegfa* transcript levels in the INL (Figure 2A), no noticeable effect was observed in the developing superficial (Supplemental Figure 3A) or deep plexus layers in P23-staged mice (Figure 2, B and C). However, the conditional deletion of *Vegfa* resulted in severe attenuation of the intermediate plexus (Figure 2B, bottom row). In order to better understand the mechanism of vascular attenuation in the *Vegfa* mutants, we quantified endothelial cell–sprouting events during key time points of intraretinal angiogenesis. The defect is not caused by inappropriate vascular sprouting from the superficial or deep plexus, or incomplete vascularization of the deep plexus (Figure 2, C–F, and Supplemental Figure 3, B–D). There were, however, significant differences in the number of branching events, the number of tip cells, and the number of filopodia on the tip cells of the sprouting vessels once they change direction and begin expanding within the intermediate plexiform layer (Figure 2, G–J). Therefore, *Vegfa* inhibition in amacrine and horizontal cells inhibits endothelial cell–sprouting in the IPL and prevents normal vascularization (Figure 2K and Supplemental Figure 4).

Vegfa gain-of-function in amacrine and horizontal cells induces massive neovascularization in the INL and IPL. We also performed gain-of-function assays for VEGF in amacrine and horizontal cells by crossing *Ptf1a-Cre* mice with floxed *Vhl* (*Vhl*$^{f/f}$) mice to induce pseudohypoxia. Sprouting blood vessels in the *Vhl* mutants became diverted from their normal paths and stopped in the INL rather than continuing to the OPL (Supplemental Figure 5A). As a result, an abnormally dense and multistratified capillary network formed in the intermediate plexiform layer at the expense of the superficial and, in particular, the deep plexus layer (Figure 3, A–E, and Supplemental Figure 5B). Abnormal vessels persisted as long as 20 months (Supplemental Figure 5C), although some vascular pruning occurred and the number of branching points decreased with age (Supplemental Figure 5D). The mechanism leading to this neovascular phenotype can most likely be explained by an upregulation of nondiffusible VEGF from pseudohypoxic amacrine and horizontal cells. Quantitative PCR (qPCR) experiments in *Vhl* mutants revealed an upregulation of all 3 VEGF isoforms, with the greatest change seen in the nondiffusible isoform ($VEGF_{188}$) that strongly binds the extracellular matrix (Figure 3F). However, in P15 *Ptf1a-Cre Vegf*$^{f/f}$ mice, soluble $VEGF_{120}$ is the most dominant and abundant isoform expressed, followed by $VEGF_{164}$ (P = 0.021646 for $VEGF_{120}$, P = 0.04667 for $VEGF_{164}$, P = 0.059891 for $VEGF_{188}$; Supplemental Figure 3E). This could indicate that membrane-bound, rather than soluble, VEGF is more important for intermediate plexus development, or that neighboring neurons upregulate soluble VEGF to compensate for the genetic depletion. Collectively, these results indicate that VHL is required for regulating HIFs and the expression of specific VEGF isoforms at proper levels for retinal vascular patterning and maintenance.

HIF-1α/VEGF signaling is required in the IPL for development of functional neurovascular units. Since others have shown that the conditional deletion of *Hif-1α* in all retinal cells prevents formation of the intermediate plexus (5), we set out to determine if the deletion of *Hif-1α* exclusively in amacrine and horizontal cells was sufficient to phenocopy the effect. Indeed, the deletion of *Hif-1α* in amacrine and horizontal cells (*Ptf1a-Cre Vhl*$^{f/+}$ *Hif-1α*$^{f/f}$) phenocopies the intermediate plexus defects seen in both *Hif-1α* or *Vegfa* mutants at P12 (Supplemental Figure 6, A and B) and P23 (Figure

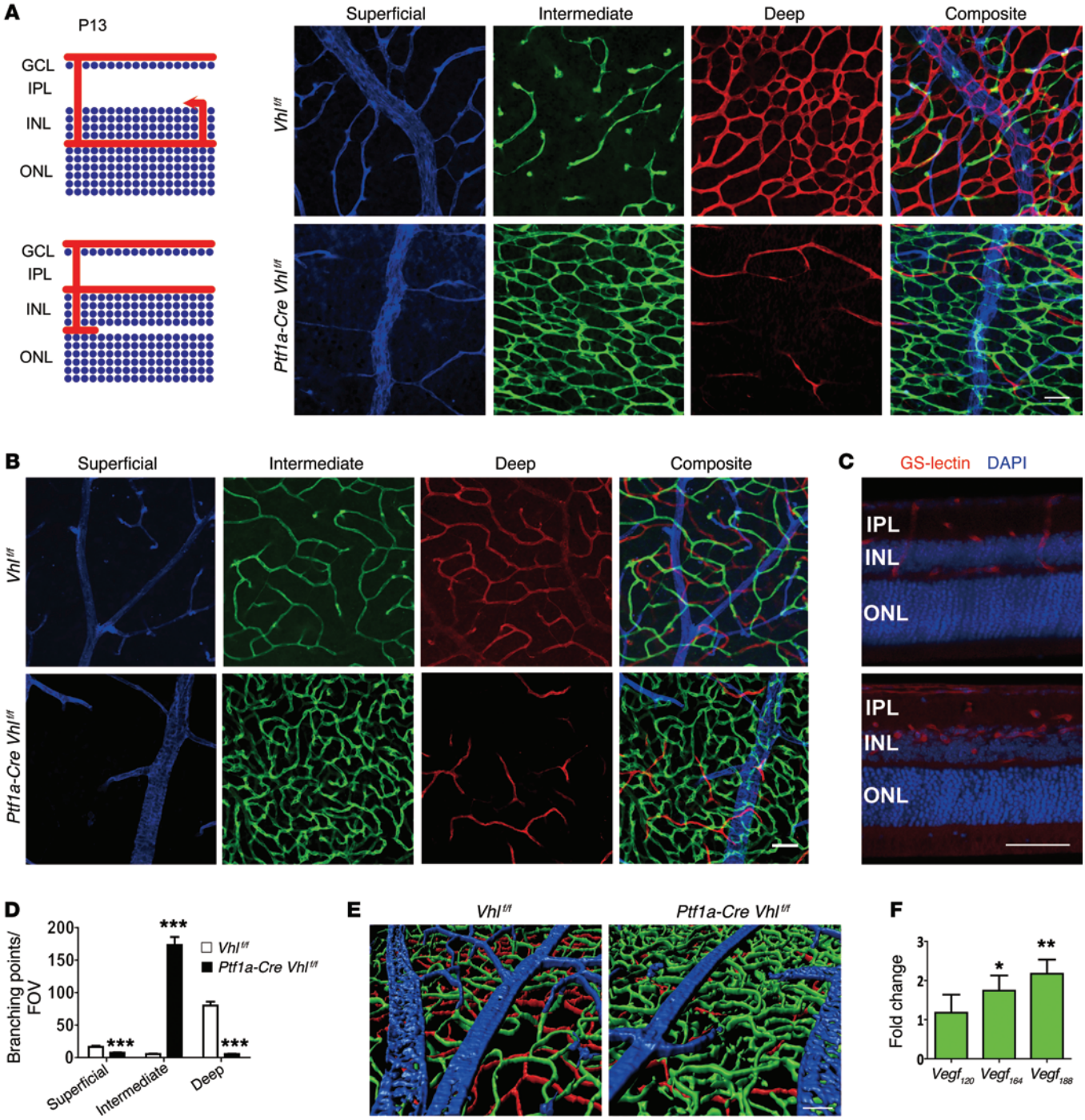

Figure 3. *Vhl* deletion in amacrine and horizontal cells induces formation of a dense and convoluted intermediate plexus at the expense of the deep plexus. (**A** and **B**) Schematic of angiogenesis in *Vhl*$^{f/f}$ (control) or *Ptf1a-Cre Vhl*$^{f/f}$ retinas at P13. Note dramatic alterations in the intermediate plexus (green) and deep plexus (red) at P13 (**A**) and P23 (**B**) in flat-mounted retinas. (**C**) 100 μm sections from P23 *Ptf1a-Cre Vhl*$^{f/f}$ mice were stained with GS-lectin to highlight the extent of the neovascularization in the VHL mutants. Counterstained with DAPI. (**D**) The number of branching events in P13 *Vhl*$^{f/f}$ or *Ptf1a-Cre Vhl*$^{f/f}$ retinas was plotted (n = 4). (**E**) Three-dimensional reconstruction of 3 retinal plexuses in P23 *Ptf1a-Cre Vhl*$^{f/f}$ retina (superficial, blue; intermediate, green; deep plexus, red) highlighted the abnormally dense intermediate plexus. (**F**) qPCR analyses revealed that nondiffusible $Vegf_{188}$ was the most abundant isoform expressed in *Ptf1a-Cre Vhl*$^{f/f}$ mice at P15 (n = 4). *P < 0.05, **P < 0.01, ***P < 0.001; 2-tailed Student's t tests. Error bars indicate mean ± SD. Scale bars: 50 μm (**A**–**C** and **E**).

4, A, B, and H). Conversely, mice lacking both copies of *Hif-2α* (*Ptf1a-Cre Vhl*$^{f/+}$ *Hif2*$^{f/f}$) appear normal (Figure 4, C and I, and Supplemental Figure 6C). *Vhl* is haplosufficient, but when both copies are deleted, *Hif-1α* and *Hif-2α* become dominantly stabilized and *Vegfa* is overexpressed. The deletion of *Hif-1α* and both *Vhl* alleles (*Ptf1a-Cre Vhl*$^{f/f}$ *Hif-1α*$^{f/f}$) prevented the formation of the unusually dense capillary bed seen in *Vhl* mutants, but the deletion of *Hif-2α* and *Vhl* (*Ptf1a-Cre Vhl*$^{f/f}$ *Hif-2α*$^{f/f}$) did not (Figure 4, D–F, J, and

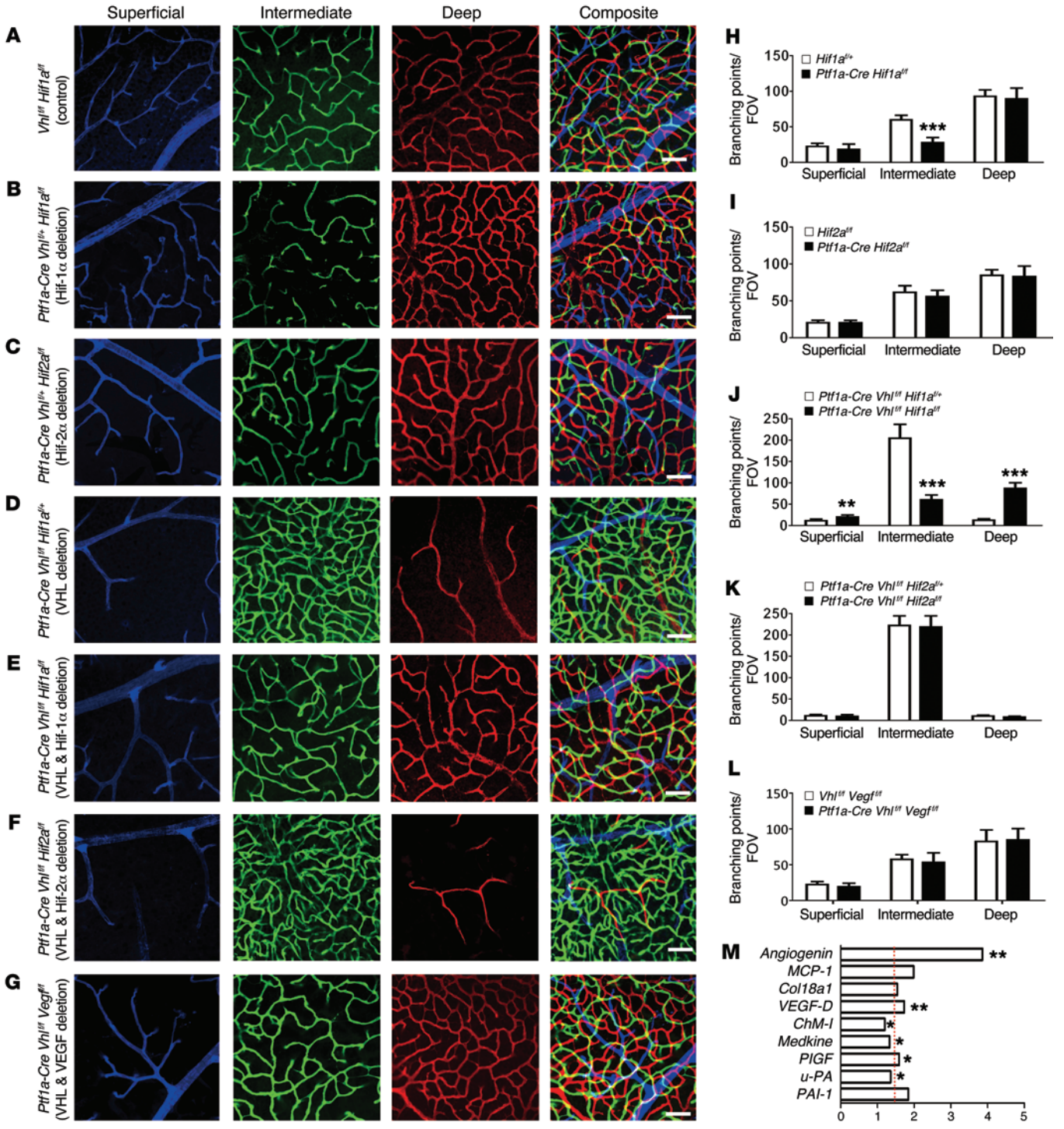

Figure 4. VHL/HIF-1α/VEGF signaling regulates angiogenesis in the intermediate plexus. (**A**–**F**) Compared with control (**A**), combinatorial conditional KO strategies were employed to show that the loss of HIF-1α (**B**; quantified in **H**) but not HIF-2α (**C**; quantified in **I**) in amacrine and horizontal cells interferes with intermediate plexus development in haplosufficient P23 *Vhl*$^{+/-}$ mutants. (**D**–**F**) Homozygous deletion of P23 *Vhl* and *Hif-1α* (**E**) prevents the neovascularization observed in *Vhl* mutants (**D** and **E**; quantified in **J**), but deletion of *Hif-2α* elicits no effect (**F**; quantified in **K**) compared with controls (**D**). (**G**; quantified in **L**) Homozygous deletion of *Vhl* and *Vegfa* also rescues the *Vhl* neovascular phenotype. (All assays were performed in P23-staged mice; $n = 4–6$). (**M**) Relative mRNA expression values from qPCR gene-profiling analysis of 84 angiogenesis-related genes in *Ptf1a-Cre Vhl*$^{f/f}$ *Vegf*$^{f/f}$ retinas at P12 compared with controls (harboring floxed alleles but no Cre); upregulated genes ($P < 0.05$ or fold change > 1.5 [marked by red dashed line]) are plotted ($n = 4$). *$P < 0.05$, **$P < 0.01$, ***$P < 0.001$; 2-tailed Student's *t* tests. Error bars indicate mean ± SD. Scale bars: 50 μm (**A**–**G**).

K, and Supplemental Figure 6, D–F). These genetic perturbations all result in spatial changes in *Vegfa* expression (Supplemental Figure 6, H–J), and collectively suggest that carefully regulated VHL/HIF-1α signaling is imperative for development of neurovascular units in the intermediate plexus.

To determine whether the neovascularization in the intermediate plexus is regulated by HIF-mediated VEGF activation, we generated *Ptf1a-Cre Vhl$^{f/f}$ Vegf$^{f/f}$* mice. Interestingly, despite observing a clear reduction in *Vegfa* expression using in situ hybridization, no obvious differences were observed in the vascular density of the intermediate plexus at P12 and P23 in *Ptf1a-Cre Vhl$^{f/f}$ Vegf$^{f/f}$* and control littermates (*Vhl$^{f/f}$ Vegf$^{f/f}$*) (Figure 4, G and L, and Supplemental Figure 6, G and K). Gene-profiling experiments in *Ptf1a-Cre Vhl$^{f/f}$ Vegf$^{f/f}$* and *Vhl$^{f/f}$ Vegf$^{f/f}$* mice revealed that other proangiogenic factors are upregulated in the mutants (Figure 4M and Supplemental Figure 6L). *Vegfa^{188}* is also upregulated in *Ptf1a-Cre Vhl$^{f/f}$ Vegf$^{f/f}$* mice compared with controls (Supplemental Figure 6M).

Genetic ablation of amacrine and horizontal cells phenocopies the effects of Vegfa deletion. To confirm that amacrine and horizontal cells can regulate development of the intraretinal vasculature, we performed genetic techniques designed to selectively ablate both cell types. This was accomplished by crossing *Ptf1a-Cre* mice with a mouse strain in which the human diphtheria toxin receptor (iDTR) is knocked into the *ROSA26* locus (*R26^{iDTR}*) (Supplemental Figure 7A). Using this technique, inducible and selective genetic ablation of 82.4% of amacrine cells (89.3 ± 17.8/0.1mm^2 in controls vs. 15.7 ± 4.9/0.1mm^2 in mutants) and 87.9% of horizontal cells (4.5 ± 1.1/0.1mm^2 in controls vs. 0.5 ± 0.5/0.1mm^2 in mutants), and a significant decrease in synaptic density in the IPL, occurred 10 days after diphtheria toxin (DT) administration (Figure 5, A–E). The reduction in the number of amacrine cells induced profound attenuation of the intermediate plexus, but not of the superficial or deep plexuses, compared with controls (Figure 5, F and G). The same phenomenon was observed when amacrine or horizontal cells were ablated starting at P6, before formation of the deep plexus (Supplemental Figure 7, B–G). We also induced ablation in adult mice and examined the vasculature 3 months after DT administration. In adult mice, we observed a significant decrease in vascular density in the intermediate plexus, but not in the superficial or deep plexuses, indicating a role for vascular maintenance and not just development (Figure 5, H and I). We also recorded light responsiveness (a-waves and b-waves) in DT-treated *Ptf1a-Cre R26$^{iDTR/+}$* and *Ptf1a-Cre R26$^{+/+}$* mice. Functional analyses using full-field electroretinography (ERG) revealed a significant reduction in the b-waves (negative ERG) of *Ptf1a-Cre R26$^{iDTR/+}$* mice (Supplemental Figure 7H), collectively indicating that amacrine cells are required for both development and maintenance of the intermediate plexus, and for propagation of the rod- and cone-driven pathways in adult stages.

Intermediate plexus abnormalities are associated with loss of visual acuity. To determine the importance of neurovascular units in the IPL for visual function, ERGs were performed on the *Vegfa* or *Vhl* mutants to measure the integrity of the photoreceptors (negative a-wave) and of the second- and third-order neurons (positive b-wave) in either dark-adapted (scotopic) or light-adapted (photopic) animals. Significant reductions of both scotopic (rod-driven) and photopic (cone-driven) responses (Figure 6A), and significantly reduced optokinetic reflexes were observed in *Ptf1a-Cre Vegf$^{f/f}$* mice (Supplemental Figure 8). Significant reductions in scotopic (rod-driven) responses were also detected in *Ptf1a-Cre Vhl$^{f/f}$* mice (Figure 6B). Importantly, neither manipulation induced neurovascular uncoupling in the INL (Supplemental Figure 9). TUNEL assays, basic ultrastructural examinations, blood tests, weight measurements, and immunohistochemistry in longitudinally monitored mutant mice showed no obvious evidence of increased cell death, neuronal development/synaptic densities, or changes to the diabetic status of the mutants, since *Ptf1a-Cre* is active in the pancreas (Supplemental Figures 10–12). Collectively, these results suggest that either attenuated or potentiated amacrine cell– and horizontal cell–derived VEGF expression disrupts vision.

Finally, *Ptf1a-Cre Vegf$^{f/f}$* mice were crossed with a retinal degeneration 10 (rd10) mouse line (*Pde6b$^{rd10/rd10}$*), which is a widely used model of photoreceptor atrophy. To quantify the degree of photoreceptor degeneration in rd10 mice with attenuated intermediate plexuses, we measured the thickness of the outer nuclear layer (ONL) in histological sections and performed TUNEL staining. At the earliest time point of retinal degeneration, P21, the number of TUNEL-positive cells was significantly increased (Figure 6, C and D) and ONL thickness was significantly thinner at 6 positions in the retina of *Ptf1a-Cre Vegf$^{f/f}$ Pde6b$^{rd10/rd10}$* mice compared with controls (*Vegf$^{f/f}$ Pde6b$^{rd10/rd10}$* and *Ptf1a-Cre Vegf$^{f/f}$ Pde6b$^{rd10/+}$* mice) (Figure 6E and Supplemental Figure 13, A–C), indicating that degeneration is accelerated in mice with impaired intermediate plexuses (Supplemental Figure 13D). These findings highlight a critical role for amacrine cells, promoting photoreceptor homeostasis and function through vascular maintenance of the intermediate plexus.

Discussion

There is mounting evidence that retinal neurons, including ganglion cells and photoreceptors, act as oxygen and nutrient sensors that can drive and regulate angiogenesis; ganglion cells can even act as rheostats to fine tune VEGF availability (3, 4, 17). However, the roles of other neurons to facilitate growth and maintenance of the deep retinal vascular layers are not completely understood. Oxygen consumption increases at distinct time points during development as neurons are born and mature. This results in localized zones of hypoxia in the developing retina. In P15-staged rats (just prior to eye opening), the intermediate vascular plexiform layer is underdeveloped and oxygen consumption is very low in the inner retina (18). During these stages of mouse development, HIF-1α levels are very high in the retina (6, 8) and VEGF is broadly, albeit transiently, detectable throughout the INL (19). Earlier reports suggested that Müller glia were the primary source of VEGF in the inner retina (19); however, conditional deletion of *Vegfa* in Müller glia cells did not affect the vasculature (20). In this study, we used genetic ablation strategies to show that amacrine cell–derived VEGF (perhaps more specifically $VEGF_{188}$) is essential for regulating intermediate plexus development, although other factors including adrenomedullin, angiogenin, or EPO may also contribute. This conclusion is based on the observation that interactions between amacrine cells and the capillaries are extensive, and that *Vegfa* loss-of-function and gain-of-function assays using *Ptf1a-Cre* result in attenuation or neovascularization of the intermediate plexus (at the expense of the deep plexus).

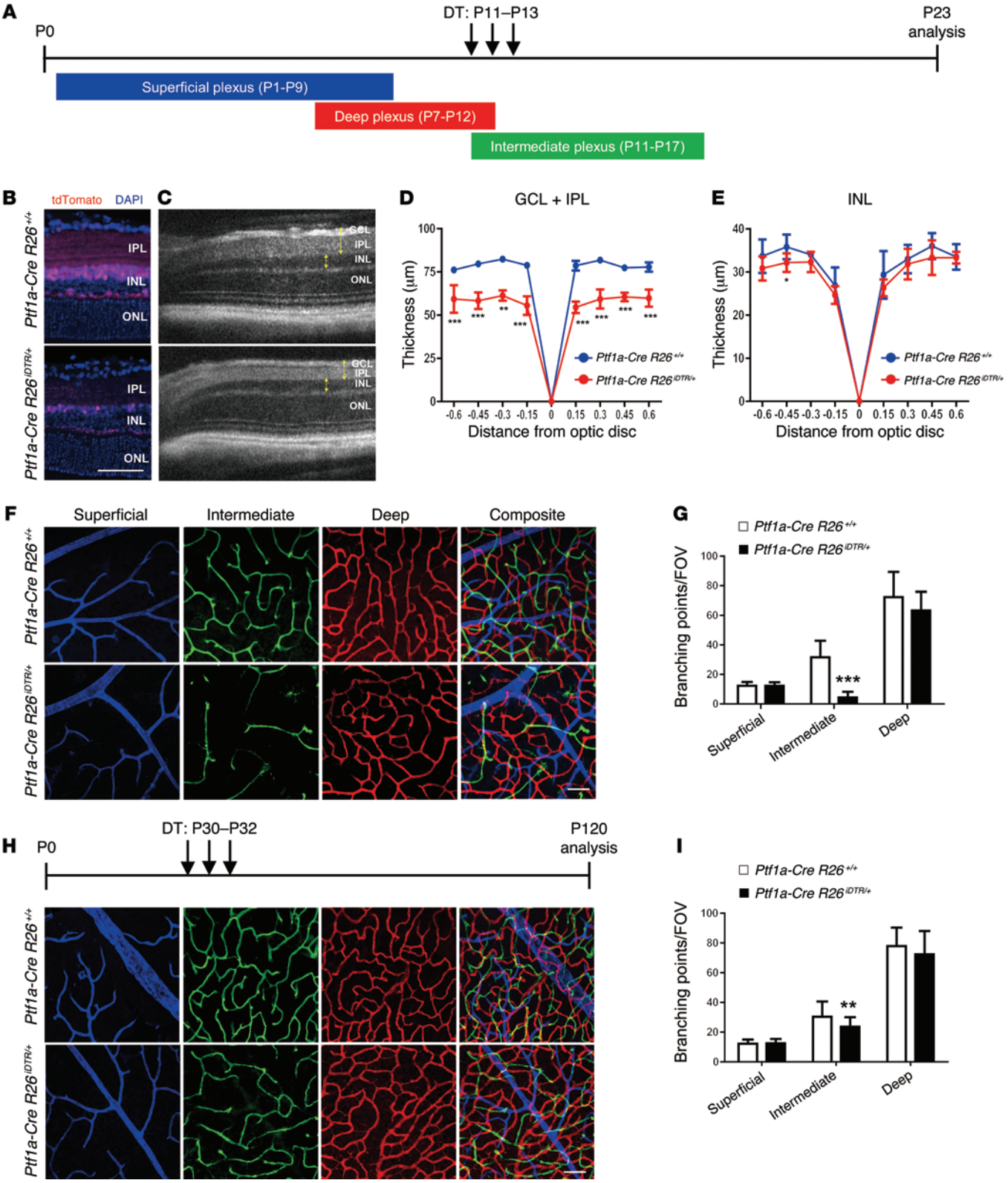

Figure 5. Genetic ablation of amacrine and horizontal cells phenocopies the defects in the intermediate plexus observed in *Hif-1α* and *Vegfa* mutants. (**A**) DT was injected daily at the time points indicated. (**B**–**E**) The reduced number of cells after ablation was examined by comparing cryosectioned retinas from P23 *Ptf1a-Cre R26*$^{iDTR/+:tdTomato/+}$ and P23 *Ptf1a-Cre R26*$^{+/+:tdTomato/+}$ mice after injecting DT (**B**), and by measuring the thickness of the GCL/IPL and INL (**C**; yellow brackets) from images captured in vivo using SD-OCT (**D** and **E**) (n = 4–6). (**F** and **G**) An attenuated intermediate plexus is observed (**F**; green) and quantified (**G**) in P23 *Ptf1a-Cre R26*$^{iDTR/+}$ mice (n = 6). (**H** and **I**) An attenuated intermediate plexus is also seen when amacrine and horizontal cells are ablated well after intermediate plexus development (**H**; quantified in **I**), suggesting that amacrine cells are required for development and maintenance of the intermediate plexus (n = 4). *P < 0.05, **P < 0.01, ***P < 0.001; 2-tailed Student's t tests. Error bars indicate mean ± SD. Scale bar: 50 μm (**B**, **F**, and **H**).

The onset of hypoxia and intermediate plexus formation in the INL correlates well temporally with the timing of synaptogenesis and the maturation of amacrine cells. At P10–P12 stages in mice (a few days prior to eye opening), when the intermediate plexus forms, all of the key events of synaptogenesis have been initiated. Amacrine cells are properly sublaminated but are still actively remodeling their lateral connections to form mature circuits. This occurs as the amacrine cells disassemble their immature cholinergic networks and generate mature ionotropic glutamate–based synapses. As the density and size of the IPL increases and the metabolic demands change, HIF-1α/VEGF signaling in amacrine cells drives angiogenesis from the deep plexus. Perturbations to VEGF signaling through *Ptf1a-Cre*–induced *Vhl* deletion result in a highly convoluted and unusually dense intermediate plexus, since the sprouting vessels from the deep plexus are attracted to a temporally inappropriate, ectopically localized, VEGF gradient.

We report here a function for amacrine cells, generating VEGF for vascular maintenance, photoreceptor homeostasis, and visual function. Amacrine and horizontal cells were previously thought to be required only for preprocessing and integrating visual stimuli. Our findings demonstrate that dysregulated *Vegfa* expression in amacrine and horizontal cells causes retinal microvascular deficits that induce loss of visual acuity. Additionally, we have observed that photoreceptor atrophy occurred earlier and faster in 2 animal models of human retinal degeneration, one of which was presented in this paper, after deleting *Vegfa* in amacrine cells. Finally, it has been reported that in an animal model of diabetic retinopathy, VEGF inhibition increased amacrine cell apoptosis (21). These findings not only demonstrate the importance of amacrine cells, but they also add to a growing body of evidence that chronic VEGF antagonism in the eye — the preferred therapeutic strategy for treating neovascular age-related macular degeneration — could elicit substantial off-target effects, leading to visual dysfunction (22–24).

This work also shows that the attenuation of the intermediate and deep vascular plexuses negatively affects retinal physiology. This concept is supported by recent evidence suggesting that neuronal dysfunction and neurodegeneration are tightly correlated with microvascular dysfunction. Microvascular dysfunction and breakdown of the blood-retinal barrier in the retina are characteristic of retinal neurodegenerative disorders, such as retinitis pigmentosa and diabetic retinopathy (11, 25–27). IPL thinning and retinal amacrine neuronal dysfunction are observed in diabetic patients (27, 28). Attenuation of the intraretinal vasculature is also highly correlated with progression of vision loss in retinitis pigmentosa (11), and our data strongly suggest that amacrine cell loss or dysfunction and ensuing intermediate plexus attenuation can accelerate photoreceptor atrophy in a murine model of the disease. Furthermore, preclinical experiments in rodent models of retinal degeneration have provided proof-of-concept evidence that stabilization of the intraretinal vasculature can retard photoreceptor atrophy (29). Finally, in humans, efforts to rebuild or repair defective neurovascular units are being actively explored to prevent or slow neurodegeneration (1); studies like this one may inform those therapeutic strategies.

In summary, we have described a role for retinal lateral interneurons, providing critical neurotrophic support through vascular maintenance of the intermediate plexus. Learning how to therapeutically control VHL/HIF-1α/VEGF signaling in amacrine cells may represent a therapeutic intervention for treating degenerative conditions that lead to vision loss.

Methods

Mouse lines. Transgenic mice expressing Cre recombinase under *Ptf1a* (*Ptf1a-Cre* mice) (30) were mated with $Vhl^{fl/fl}$ (31), $Hif\text{-}1\alpha^{fl/fl}$ (32), or $Hif\text{-}2\alpha^{fl/fl}$ (33), $Vegf^{fl/fl}$ (16), $Pde6b^{rd10/rd10}$ (rd10), and $Rosa26^{iDTR/+}$ (C57BL/6-Gt(ROSA)26Sor$^{tm1(HBEGF)Awai}$/J) (34) mice (The Jackson Laboratory). *Ptf1a-Cre* mice were crossed with floxed *Vegf, Vhl, Hif-1α, or Hif-2α* alleles for conditional-deletion experiments. Littermate controls were used in all cases. To monitor Cre recombination in *Ptf1a-Cre* mice, we mated them with 2 different reporters: ROSA26tm14(CAG-tdTomato)(Ai14; ref. 35) for *Ptf1a*-specific nuclear expression and ROSA mTomato/mGFP transgenic reporter mice (14) for *Ptf1a*-specific membrane expression. We screened mice in our colony for retinal degeneration slow (rds), rd1 and rd8 mutations. Genotyping was performed by Transnetyx Inc.

Electron microscopy. For scanning electron microscopy, lightly fixed retinas (buffered paraformaldehyde) were fixed overnight in 2.5% glutaraldehyde in 0.1M Na cacodylate buffer pH 7.4. Cross sections were prepared with a #11 scalpel blade, then washed with buffer, postfixed in 1% osmium tetroxide, washed in 0.1 M cacodylate buffer, washed with distilled water, and then dehydrated in series of graded ethanol. The tissues were then treated with hexamethyldisilazane (HMDS) (Electron Microscopy Sciences) as a substitute for critical point drying, dried and mounted onto SEM stubs with carbon tape, and sputter coated with 4nm of Iridium (EMS model 150T S) for examination on a Hitachi S-4800 SEM (Hitachi). For transmission electron microscopy, the analysis was carried out as described previously (23). Eye cups were fixed in 4% paraformaldehyde plus 1.5% glutaraldehyde in 0.1 M sodium cacodylate buffer overnight at 4°C, followed by rinsing in 0.1 M Na cacodylate buffer for 1 hour. Eye cups were postfixed in 1% osmium tetroxide in 0.1 M Na cacodylate buffer for 2 hours, then dehydrated in graded ethanol solutions. The tissues were incubated overnight in a 1:2 mixture of propylene oxide and Epon/Araldite (Sigma-Aldrich) and placed in 100% resin, followed by embedding. The blocks were sectioned and used for high-magnification electron microscopy analysis.

In vivo imaging. The fundus images of mice were captured using a Micron III platform (Phoenix Research Laboratories). SD-OCT was performed using an Envisu device (Bioptigen). Averaged SD-OCT scans were exported to Adobe Photoshop CS6 (Adobe Systems Inc.) for quantitative analysis. Manual segmentation using the Adobe Photoshop CS6 ruler instrument was used to accurately measure retinal layers (ganglion cell layer [GCL]/IPL and INL). The different retinal layers were plotted in ± 15 mm increments for up to ± 60 mm from the optic nerve head. Mice were anesthetized by intraperitoneal injection of 15 mg/kg ketamine and 7 mg/kg xylazine, and perfused with indocyanine green (ICG) (50 μg/g body weight). Pupils were dilated with 1% tropicamide and 2.5% phenylephrine immediately prior to imaging.

Immunofluorescence. Whole-mount preparations were performed after removing the cornea, lens, retina pigment epithelium, choroid, and sclera as previously described (36, 37). Immunostaining of cryosections or vibratome sections (100 μm) was carried out as previously described (36). The following primary antibodies were used in this study: CD31 (catalog 553370, BD Biosciences), calbindin D-28K (catalog AB1778, Millipore), synaptophysin1 (catalog 101 011, Synap-

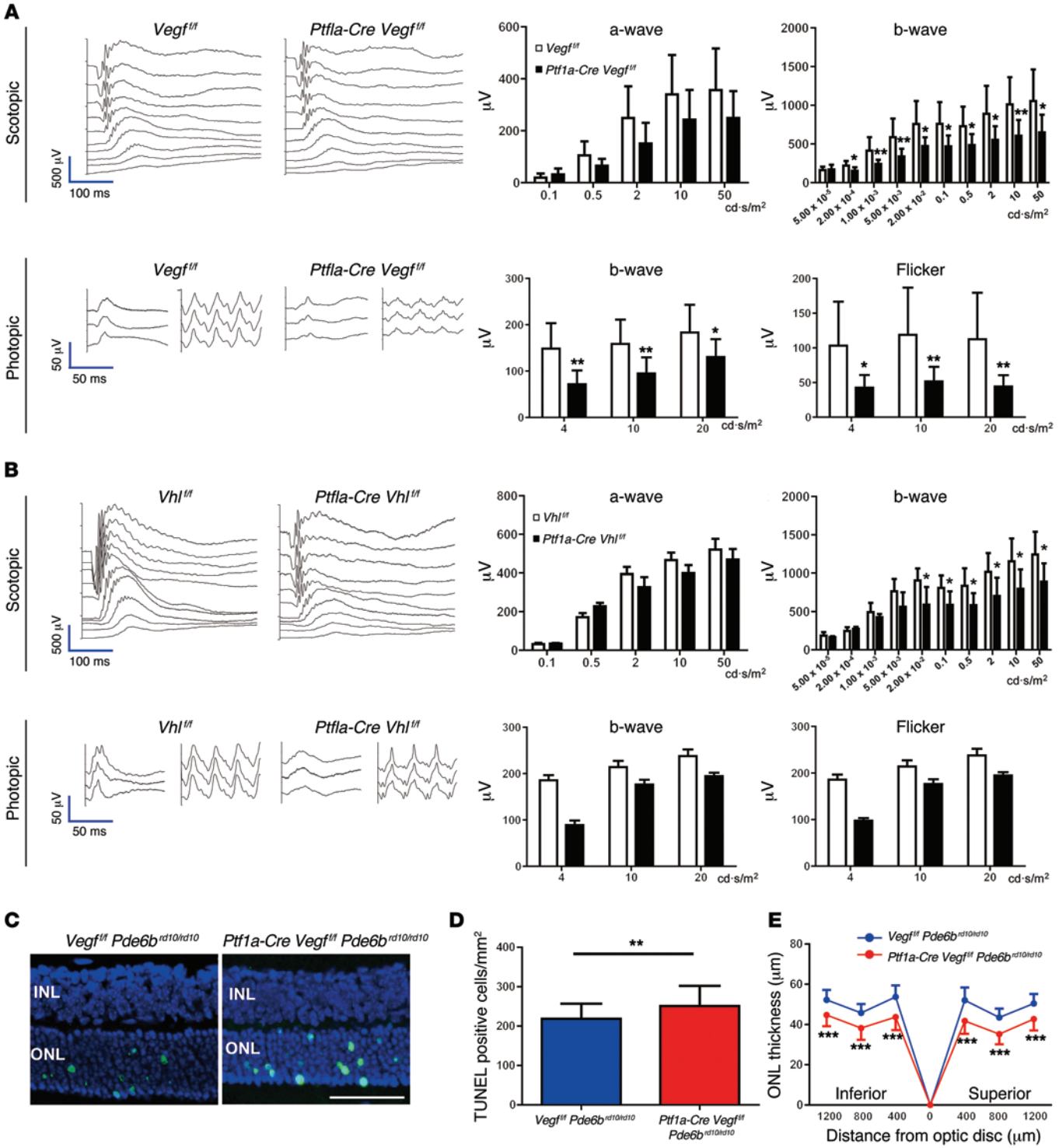

Figure 6. Intermediate plexus abnormalities are associated with visual dysfunction. (**A**) Full-field ERGs in 2-month-old *Ptf1a-Cre Vegf*$^{f/f}$ mice reveal significant defects in both rod- and cone-driven pathways (n = 8–10). (**B**) Full-field ERGs performed on 2-month-old *Ptf1a-Cre Vhl*$^{f/f}$ mice reveal that the rod-driven pathways are significantly impaired (n = 6). (**C**–**E**) Photoreceptor atrophy is accelerated in a mouse model of spontaneous retinal degeneration (rd10 mice) with impaired intermediate plexuses, based on TUNEL staining in the ONL (**C**; green, quantified in **D**), and reduced ONL thickness values (**E**) in P21 *Ptf1a-Cre Vegf*$^{f/f}$ *Pde6b*$^{rd10/rd10}$ mice and controls (*Vegf*$^{f/f}$ *Pde6b*$^{rd10/rd10}$; n = 6 each). *P < 0.05, **P < 0.01, ***P < 0.001; 2-tailed Student's t tests. Error bars indicate mean ± SD. Scale bar: 50 µm.

tic Systems), calretinin (catalog 7697, Swant), glutamine synthetase (catalog PA1-46165, GS-6, ThermoScientific), chx10 (catalog X1179P, Exalpha Biologies Inc.), NF-M (2H3, Developmental Studies Hybridoma Bank) (38), MAP2 (catalog NB300-213, Novus Biologicals), rabbit polyclonal GFP (catalog A21311, Invitrogen), glycine transporter 1 (catalog AB1770, Millipore), STX1 (catalog S0664, Sigma-Aldrich), and glutamate decarboxylase 65 and 67 (catalog AB1511, Millipore). Fluorescence-conjugated isolectin *Griffonia simplicifolia*

IB-4 was also used (GS-lectin; catalog I21413, Invitrogen). The retinas and sections were incubated with the corresponding Alexa Fluor-conjugated secondary antibodies (Invitrogen), and nuclei were stained with DAPI (Vector Laboratories).

Confocal microscopy and quantification. All images were acquired with a confocal laser-scanning microscope (LSM 700 or 710, Zeiss) and processed with the ZEN 2010 software (Zeiss). Three-dimensional reconstructions were generated using ZEN 2010 and Imaris software (Bitplane). The quantification of cells or substances of interest was performed as previously described (37, 39). In brief, to assess the density of the vascular plexus, eight ×200 magnification images (4 center and 4 peripheral; 320 × 320 μm fields of view [FOV] per retina) were chosen from each scanned image, and the numbers obtained from each of the 8 fields were averaged. We scored tip cells as GS-lectin–positive cells with blind-ended endothelial protrusions that had associated filopodial bursts in areas at the angiogenic front by analyzing high-magnification (×400) micrographs. To quantify numbers of filopodia per tip cell, randomly selected high-magnification (×400) micrograph images were analyzed. To construct triple-colored images, images were overlaid using Adobe Photoshop CS6.

In situ hybridization. In situ hybridizations were performed using ViewRNA ISH Tissue Assay for RNA kits (catalog QVT0013, Affymetrix) according to the manufacturer's instructions. The ISH probe for murine *Vegfa* was designed and synthesized by Affymetrix and is now commercially available (catalog SB-13465).

Gene profiling. Total RNA was isolated from the retinal tissues using miRNeasy Mini Kit (QIAGEN) and reverse transcribed using the QuantiTect Reverse Transcription Kit (QIAGEN), following the manufacturer's instructions. qPCR assays were performed using the CFX96 Touch Real-Time PCR Detection System (Bio-Rad) using a QuantiTect SYBR Green PCR Kit (QIAGEN) to quantify the mRNA expression levels of the $Vegf_{120}$, $Vegf_{164}$, and $Vegf_{188}$ isoforms using primers previously described (40). Reactions were performed in quadruplicate with β-actin as an internal control. These data were normalized to control littermates harboring floxed alleles but no Cre-recombinase. mRNA PCR array for angiogenesis (RT^2 Profiler PCR Array for Mouse Angiogenesis [PAMM-024]) or Mouse Hypoxia Signaling Pathway (PAMM-032) was used according to the manufacturer's instructions (QIAGEN). Data were analyzed with the 7900HT Fast System SDS 2.4 Software (Invitrogen).

In vivo genetic ablation studies. For in vivo genetic ablation studies, *Ptf1a-Cre* mice were crossed with *R26*$^{iDTR/+}$ mice (C57BL/6-Gt(ROSA)26Sor$^{tm1(HBEGF)Awai}$/J) (34), yielding double-transgenic *Ptf1a-Cre R26*$^{iDTR/+}$ (iDTR-positive) mice that selectively expressed iDTR in amacrine and horizontal cells. The iDTR is only expressed after Cre-mediated excision of a transcriptional STOP cassette (Supplemental Figure 5A). To achieve the phase-restricted depletion of amacrine and horizontal cells, *Ptf1a-Cre R26*$^{iDTR/+}$ and control littermates (*Ptf1a-Cre R26*$^{+/+}$ and *R26*$^{iDTR/+}$) were injected intraperitoneally for 3 consecutive days with 25 ng/g DT (Sigma-Aldrich).

TUNEL staining. TUNEL was performed using an In Situ Cell Death Detection Kit (Roche Diagnostics) according to the manufacturer's instructions. The quantification of TUNEL-positive cells was performed as previously described (41). The sections were counterstained with DAPI.

Blood glucose and HbA_{1C} measurements. The blood glucose and hemoglobin A_{1C} (HbA_{1C}) levels in the blood, which had been obtained from the mouse tail vein, were measured using the FreeStyle blood glucose monitoring system (Abbott) and the A1cNow rapid immunoassay (Bayer), respectively.

Ganzfeld ERG. ERG was performed according to procedures previously described (23, 36). Mice were dark-adapted overnight before the experiments and anesthetized under a dim red light by intraperitoneal injection of 15 mg/kg ketamine and 7 mg/kg xylazine. Silver needle electrodes served as a reference (forehead) and ground (tail). Full-field ERGs were recorded from the corneal surface of each eye after pupil dilation (with 2.5% phenylephrine and 1% tropicamide) with active contact lens electrodes (Mayo). A computerized system with an electronically controlled Ganzfeld dome was used (Espion E2 with Colordome; Diagnosys). In the dark-adapted condition (scotopic), we recorded rod and mixed cone/rod responses to a series of white flashes of increasing intensities (1×10^{-5} to 50 cd·s/m^2). In the light-adapted condition (photopic), with a 30 cd/m^2 background, cone responses to 1-Hz (0.63 to 20 cd·s/m^2) and 30-Hz (3.98, 10, and 20 cd·s/m^2) flicker stimuli were recorded. All ERG responses were filtered at 0.3-500 Hz, and signal averaging was applied.

Evaluation of visual acuity. Visual acuity of the mice was assessed by the optokinetic response using the OptoMotry system (CerebralMechanics Inc.) according to procedures previously described (42).

Statistics. Comparison between the average variables of the 2 groups was performed by 2-tailed Student's *t* test. *P* values < 0.05 were considered statistically significant.

Study approval. All animal experiments were carried out in accordance with the Scripps Research Institute's IACUC protocols.

Acknowledgments

We would like to thank Malcolm R. Wood, Lea Scheppke, Lindsay Keir, Stephen Bravo, and Mauricio Rosenfeld for technical assistance and critical discussions of the data, and Randall S. Johnson at University of Cambridge for providing transgenic mice. This work was supported by grants to M. Friedlander from the National Eye Institute (R01 EY11254 and R24 EY022025) and the Lowy Medical Research Foundation (MacTel). Y. Usui is supported by a fellowship from the Manpei Suzuki Diabetes Foundation and the Alcon Japan Hida Memorial Award.

Address correspondence to: Martin Friedlander, The Scripps Research Institute, MB 28, 10550 North Torrey Pines Road, La Jolla, California, USA. Phone: 858.784.9138; E-mail: friedlan@scripps.edu.

1. Storkebaum E, Quaegebeur A, Vikkula M, Carmeliet P. Cerebrovascular disorders: molecular insights and therapeutic opportunities. *Nat Neurosci*. 2011;14(11):1390–1397.
2. Stanimirovic DB, Friedman A. Pathophysiology of the neurovascular unit: disease cause or consequence? *J Cereb Blood Flow Metab*. 2012;32(7):1207–1221.
3. Sapieha P. Eyeing central neurons in vascular growth and reparative angiogenesis. *Blood*. 2012;120(11):2182–2194.
4. Fruttiger M. Development of the retinal vasculature. *Angiogenesis*. 2007;10(2):77–88.
5. Caprara C, Thiersch M, Lange C, Joly S, Samardzija M, Grimm C. HIF1A is essential for the development of the intermediate plexus of the retinal vasculature. *Invest Ophthalmol Vis Sci*. 2011;52(5):2109–2117.
6. Grimm C, et al. Neuroprotection by hypoxic preconditioning: HIF-1 and erythropoietin protect from retinal degeneration. *Semin Cell Dev Biol*.

2005;16(4-5):531–538.
7. Yu DY, Yu PK, Cringle SJ, Kang MH, Su EN. Functional and morphological characteristics of the retinal and choroidal vasculature. *Prog Retin Eye Res*. 2014;40:53–93.
8. Nakamura-Ishizu A, et al. The formation of an angiogenic astrocyte template is regulated by the neuroretina in a HIF-1-dependent manner. *Dev Biol*. 2012;363(1):106–114.
9. Dorrell MI, Aguilar E, Scheppke L, Barnett FH, Friedlander M. Combination angiostatic therapy completely inhibits ocular and tumor angiogenesis. *Proc Natl Acad Sci U S A*. 2007;104(3):967–972.
10. Stone J, Dreher Z. Relationship between astrocytes, ganglion cells and vasculature of the retina. *J Comp Neurol*. 1987;255(1):35–49.
11. Ma Y, et al. Quantitative analysis of retinal vessel attenuation in eyes with retinitis pigmentosa. *Invest Ophthalmol Vis Sci*. 2012;53(7):4306–4314.
12. Stahl A, et al. The mouse retina as an angiogenesis model. *Invest Ophthalmol Vis Sci*. 2010;51(6):2813–2826.
13. Fujitani Y, et al. Ptf1a determines horizontal and amacrine cell fates during mouse retinal development. *Development*. 2006;133(22):4439–4450.
14. Muzumdar MD, Tasic B, Miyamichi K, Li L, Luo L. A global double-fluorescent Cre reporter mouse. *Genesis*. 2007;45(9):593–605.
15. Chien CL, Liem RK. The neuronal intermediate filament, alpha-internexin is transiently expressed in amacrine cells in the developing mouse retina. *Exp Eye Res*. 1995;61(6):749–756.
16. Gerber HP, et al. VEGF is required for growth and survival in neonatal mice. *Development*. 1999;126(6):1149–1159.
17. Okabe K, et al. Neurons limit angiogenesis by titrating VEGF in retina. *Cell*. 2014;159(3):584–596.
18. Cringle SJ, Yu PK, Su EN, Yu DY. Oxygen distribution and consumption in the developing rat retina. *Invest Ophthalmol Vis Sci*. 2006;47(9):4072–4076.
19. Stone J, et al. Development of retinal vasculature is mediated by hypoxia-induced vascular endothelial growth factor (VEGF) expression by neuroglia. *J Neurosci*. 1995;15(7):4738–4747.
20. Bai Y, et al. Muller cell-derived VEGF is a significant contributor to retinal neovascularization. *J Pathol*. 2009;219(4):446–454.
21. Park HY, Kim JH, Park CK. Neuronal cell death in the inner retina and the influence of vascular endothelial growth factor inhibition in a diabetic rat model. *Am J Pathol*. 2014;184(6):1752–1762.
22. Grunwald JE, et al. Risk of geographic atrophy in the comparison of age-related macular degeneration treatments trials. *Ophthalmology*. 2014;121(1):150–161.
23. Kurihara T, Westenskow PD, Bravo S, Aguilar E, Friedlander M. Targeted deletion of Vegfa in adult mice induces vision loss. *J Clin Invest*. 2012;122(11):4213–4217.
24. Saint-Geniez M, Kurihara T, Sekiyama E, Maldonado AE, D'Amore PA. An essential role for RPE-derived soluble VEGF in the maintenance of the choriocapillaris. *Proc Natl Acad Sci U S A*. 2009;106(44):18751–18756.
25. Vinores SA, et al. Blood-retinal barrier breakdown in retinitis pigmentosa: light and electron microscopic immunolocalization. *Histol Histopathol*. 1995;10(4):913–923.
26. Klaassen I, Van Noorden CJ, Schlingemann RO. Molecular basis of the inner blood-retinal barrier and its breakdown in diabetic macular edema and other pathological conditions. *Prog Retin Eye Res*. 2013;34:19–48.
27. Stem MS, Gardner TW. Neurodegeneration in the pathogenesis of diabetic retinopathy: molecular mechanisms and therapeutic implications. *Curr Med Chem*. 2013;20(26):3241–3250.
28. Barber AJ, Lieth E, Khin SA, Antonetti DA, Buchanan AG, Gardner TW. Neural apoptosis in the retina during experimental and human diabetes. Early onset and effect of insulin. *J Clin Invest*. 1998;102(4):783–791.
29. Otani A, et al. Rescue of retinal degeneration by intravitreally injected adult bone marrow-derived lineage-negative hematopoietic stem cells. *J Clin Invest*. 2004;114(6):765–774.
30. Kawaguchi Y, Cooper B, Gannon M, Ray M, MacDonald RJ, Wright CV. The role of the transcriptional regulator Ptf1a in converting intestinal to pancreatic progenitors. *Nat Genet*. 2002;32(1):128–134.
31. Haase VH, Glickman JN, Socolovsky M, Jaenisch R. Vascular tumors in livers with targeted inactivation of the von Hippel-Lindau tumor suppressor. *Proc Natl Acad Sci U S A*. 2001;98(4):1583–1588.
32. Ryan HE, et al. Hypoxia-inducible factor-1alpha is a positive factor in solid tumor growth. *Cancer Res*. 2000;60(15):4010–4015.
33. Gruber M, Hu CJ, Johnson RS, Brown EJ, Keith B, Simon MC. Acute postnatal ablation of Hif-2alpha results in anemia. *Proc Natl Acad Sci U S A*. 2007;104(7):2301–2306.
34. Buch T, et al. A Cre-inducible diphtheria toxin receptor mediates cell lineage ablation after toxin administration. *Nat Methods*. 2005;2(6):419–426.
35. Madisen L, et al. A robust and high-throughput Cre reporting and characterization system for the whole mouse brain. *Nat Neurosci*. 2010;13(1):133–140.
36. Westenskow PD, et al. Ras pathway inhibition prevents neovascularization by repressing endothelial cell sprouting. *J Clin Invest*. 2013;123(11):4900–4908.
37. Kurihara T, et al. von Hippel-Lindau protein regulates transition from the fetal to the adult circulatory system in retina. *Development*. 2010;137(9):1563–1571.
38. Alvarez-Bolado G, Zhou X, Voss AK, Thomas T, Gruss P. Winged helix transcription factor Foxb1 is essential for access of mammillothalamic axons to the thalamus. *Development*. 2000;127(5):1029–1038.
39. Kubota Y, et al. M-CSF inhibition selectively targets pathological angiogenesis and lymphangiogenesis. *J Exp Med*. 2009;206(5):1089–1102.
40. Zhang L, et al. Different effects of glucose starvation on expression and stability of VEGF mRNA isoforms in murine ovarian cancer cells. *Biochem Biophys Res Commun*. 2002;292(4):860–868.
41. Murakami Y, et al. Receptor interacting protein kinase mediates necrotic cone but not rod cell death in a mouse model of inherited degeneration. *Proc Natl Acad Sci U S A*. 2012;109(36):14598–14603.
42. Prusky GT, Alam NM, Beekman S, Douglas RM. Rapid quantification of adult and developing mouse spatial vision using a virtual optomotor system. *Invest Ophthalmol Vis Sci*. 2004;45(12):4611–4616.